Crystal chemistry of natural layered double hydroxides. 5. Single-crystal structure refinement of hydrotalcite, $[Mg_6Al_2(OH)_{16}](CO_3)(H_2O)_4$

ZHITOVA E.S.[1,*], KRIVOVICHEV S.V.[1,2], PEKOV I.V.[3] AND GREENWELL H.C.[4]

[1] Department of Crystallography, Institute of Earth Sciences, St. Petersburg State University, St. Petersburg, Russia, e.zhitova@spbu.ru

[2] Nanomaterials Research Centre, Kola Science Centre, Russian Academy of Sciences, Apatity, Russia

[3] Department of Mineralogy, Faculty of Geology, Moscow State University, Moscow, Russia

[4] Department of Earth Sciences, Durham University, Durham, UK, DH1 3LE

*E-mail: zhitova_es@mail.ru

[*Received 8 May 2018; Accepted 3 July 2018; Associate Editor: Anthony Kampf*]

Mineralogical Society

This is a 'preproof' accepted article for Mineralogical Magazine. This version may be subject to change during the production process.
DOI: 10.1180/mgm.2018.145.

Abstract

Hydrotalcite, ideally $[Mg_6Al_2(OH)_{16}](CO_3)(H_2O)_4$, was studied in samples from Dypingdal, Snarum, Norway (3*R* and 2*H*), Zelentsovskaya pit (2*H*) and Praskovie-Evgenievskaya pit (2*H*) (both Southern Urals, Russia), Talnakh, Siberia, Russia (3*R*), Khibiny, Kola, Russia (3*R*), and St. Lawrence, New York, USA (3*R* and 2*H*). Two polytypes, 3*R* and 2*H* (both "classical"), were confirmed on the basis of single-crystal and powder X-ray diffraction data. Their chemical composition was studied by electron-microprobe analysis, infrared spectroscopy, differential scanning calorimetry, and thermogravimetric analysis. The crystal structure of hydrotalcite-3*R* was solved by direct methods in the space group *R*-3*m* on three crystals (two data collections at 290 K and one at 120 K). The unit-cell parameters are as follows (290/290/120 K): a = 3.0728(9)/ 3.0626(3)/ 3.0617(4), c = 23.326(9)/ 23.313(3) / 23.203(3)Å, V = 190.7(1)/ 189.37(4)/ 188.36(4) Å^3). The crystal structures were refined on the basis of 304/150/101 reflections to R_1 = 0.075/0.041/0.038. Hydrotalcite-2*H* crystallizes in the $P6_3/mmc$ space group, unit-cell parameters for two crystals are (data collection at room temperature and 93 K): a = 3.046(1)/ 3.0521(9), c = 15.447(6)/ 15.439(4) Å, V = 124.39(8)/ 124.55(8) Å^3. The crystal structures were refined on the basis of 160/ 142 reflections to R_1 = 0.077/ 0.059. The paper reports the first single-crystal structure data on hydrotalcite. Hydrotalcite distribution in nature, diagnostic features, polytypism, interlayer topology and localization of M^{2+}-M^{3+} cations within metal hydroxide layers are discussed.

KEYWORDS: hydrotalcite, crystal structure, natural layered double hydroxide.

Introduction

Hydrotalcite, ideally $[Mg_6Al_2(OH)_{16}](CO_3)(H_2O)_4$, is the archetype of the hydrotalcite-supergroup minerals, which are also known as natural layered double hydroxides (LDHs). This supergroup now includes more than forty structurally and chemically related species (Mills *et al*., 2012a). The mineral hydrotalcite has been known since 1842, when it was first described by Hochstetter (1842) in material from the Dypingdal serpentine-magnesite deposit in Snarum (Modum, Buskerud, Norway). As well as existing as minerals, LDHs are often prepared synthetically, owing to their wide range of useful properties (Evans and Slade, 2006).

Crystal structures of the hydrotalcite-supergroup minerals consist of positively charged brucite-type layers with octahedral sites occupied by M^{2+} and M^{3+} cations; in the currently known minerals, species-defining M^{2+} are Mg, Fe, Mn, Ni, Cu, Ca, Zn and M^{3+} = Al, Fe, Mn, Co and Cr. The octahedral layers alternate with negatively charged interlayers occupied by $(CO_3)^{2-}$, Cl^-, $(SO_4)^{2-}$, $[Sb(OH)_6]$, OH^- ions and H_2O molecules. Hydrotalcite-group members have M^{2+}:M^{3+} = 3:1 and contain interlayer species such as carbonate or hydroxyl groups or chlorine (Mills *et al*., 2012a). The general formula of the hydrotalcite-group minerals can be written as $[M^{2+}_6M^{3+}_2(OH)_{16}]^{q+}(X^{n-})_{q/n}\cdot 4H_2O$, where M^{2+} and M^{3+} are cations and X is an anion.

The first X-ray crystallographic data on a hydrotalcite-supergroup mineral were reported for pyroaurite, $[Mg_6Fe^{3+}_2(OH)_{16}](CO_3)(H_2O)_4$ (Fe^{3+}-analogue of hydrotalcite), which was found in two polytypic modifications: 3*R* (a = 3.089, c = 23.23 Å) and 2*H* (a = 3.097, c = 15.56 Å) (Aminoff and Broomé, 1931). The polytypism of hydrotalcite was investigated by Frondel (1941), who determined the following unit-cell parameters for this mineral: a = 6.13, c = 46.15 Å for the rhombohedral form, and a = 6.12, c = 15.34 Å for the hexagonal form. The doubling of the a parameter for both polytypes and the doubling of the c parameter for the rhombohedral modification was justified by the need to obtain integral atom content in the unit cell and not by the observation of any superstructure reflections (Taylor, 1973). Later single-crystal structure refinement of "hydrotalcite" was reported by Allmann and Jepsen (1969) on a specimen from

Moravia (Czech Republic), with the formula $[Mg_4Al_2(OH)_{12}](CO_3)(H_2O)_3$. However, in the current nomenclature scheme (Mills *et al*., 2012a), this corresponds to quintinite, which differs from hydrotalcite in the M^{2+}:M^{3+} ratio (2:1 rather than 3:1). In general, quintinite and its synthetic analogues are very commonly reported as "hydrotalcite" or "hydrotalcite-like phase" in the literature. For example, the widely cited paper by Bellotto *et al*. (1996) reports the Rietveld structure refinement of quintinite, and not hydrotalcite, as the title suggests. This historic and widespread inconsistency results in some confusion into the structural systematics of a large family of LDH minerals, with ramifications for the methods of LDH synthesis. It also raises a number of questions on the relative abundance of quintinite and hydrotalcite in nature, their structural characterization and diagnostic features.

Our ongoing examination of material from many localities indicates that many specimens traditionally labeled as "hydrotalcite" in fact correspond to quintinite. There are, just in Russia, for example, samples from the Kovdor alkaline-ultrabasic complex, Kola Peninsula (Krivovichev *et al*., 2010a,b; Zhitova *et al*., 2010, 2018a), the Bazhenovskoe chrysotile-asbestos deposit (Krivovichev *et al*., 2012), and the Mariinskoe emerald and beryllium deposit, Ural Emerald Mines (Zhitova *et al*., 2018b), both in the Middle Urals.

Recently, the neotype specimen of hydrotalcite from Snarum was established by Mills *et al*. (2016), who confirmed, using powder X-ray diffraction data and electron-microprobe analyses, that this is a real hydrotalcite (M^{2+}:M^{3+} = 3:1) represented by intimate intergrowths of three-layer (rhombohedral, 3*R*) and two-layer (hexagonal, 2*H*) polytypes. The predominant phase in the neotype is a 3*R* polytype (69 %), a = 3.05(1) Å, c = 23.36(1) = 3 × 7.79 Å, whereas a 2*H* polytype is subordinate (31%), a = 3.07(1) Å, c = 15.62(5) = 2 × 7.81 Å (Mills *et al*., 2016). Powder X-ray diffraction data, including Rietveld refinement results, for synthetic Mg-Al-CO_3 LDHs were reported by Bellotto *et al*. (1996), Sharma *et al*. (2008), Cocheci *et al*. (2010), Liao *et al*. (2012) and Wang *et al*. (2013). Besides "classical" 3*R* and 2*H* polytypes, an

exotic 6*R* modification was described for hydrotalcite based on powder X-ray diffraction patterns (Stanimirova, 2001).

A challenge with the structure refinement of hydrotalcite, in particular, and LDHs in general, arises from the rarity of crystals suitable for single-crystal X-ray diffraction. While studying hydrotalcite samples from different sources (see below), we were able to select samples with satisfactory quality for single-crystal data collection and structure refinement.

In the previous four papers of the current series we discussed polytypism of quintinite focusing on the ordering of the M^{2+} and M^{3+} cations (Krivovichev *et al*., 2010a,b, Zhitova *et al*., 2010, 2018a). The present paper is intended to provide new mineralogical and crystal chemical information on hydrotalcite itself, including the first single-crystal structure data for the mineral.

Occurrence and sample description

In our collection of hydrotalcite-group minerals, hydrotalcite itself, *i.e*., the mineral corresponding to the simplified formula $[Mg_6Al_2(OH)_{16}](CO_3)(H_2O)_4$, was found in material from six localities. There are, as follows.

1. Dypingdal serpentine-magnesite deposit, Snarum, Modum, Buskerud, Norway: samples # 105371 and # 158518 (Fig. 1a) from the collections of the Smithsonian National Museum of Natural History (SNM), Washington, DC, USA, and # 52071 from the systematic collection of the Fersman Mineralogical Museum of the Russian Academy of Sciences, Moscow, Russia (FMM). Details on the geological setting of hydrotalcite from Snarum are given by Mills *et al*. (2016). The studied material is represented by aggregates of pearly-white curved, corrugated scales forming nests in a green-yellow serpentine with hematite.
2. Zelentsovskaya pit in Nazyamskie Mts., Zlatoust district, Southern Urals, Russia: # 80947 from FMM and # 10532 (Fig. 1c) from the collection of one of the authors (IVP). The detailed description of geological setting for “manasseite” from altered skarns of the

Zelentsovskaya pit was provided by Ivanov and Aizikovich (1980). Hydrotalcite is found in pseudomorphs after spinel and chondrodite associated with clinochlore, calcite, and magnetite. It forms beige to pale pink coarse-lamellar aggregates.

3. Praskovie-Evgenievskaya pit in Shishimskie Mts., Zlatoust district, Southern Urals, Russia: # 10604 from the IVP collection. The skarn mineralization of the Praskovie-Evgenievskaya pit, like the Zelentsovskaya pit, is located in the contact zone between dolomite marble and gabbro. Hydrotalcite occurs as massive, monomineral pale beige scaly aggregates, forming nests up 10 cm across.
4. Komsomol'skii Mine, Talnakh Cu-Ni deposit, Norilsk district, Krasnoyarsk Kray, Siberia Russia: # 9699 from IVP collection (Fig. 1b). Hydrotalcite is found in cavities in the axial part of a calcite veinlet cross-cutting a chalcopyrite-pyrrhotite orebody. The mineral forms transparent, colourless tabular hexagonal crystals up to 1 mm across on calcite and is associated with valleriite.
5. St. Lawrence, New York, USA. The studied sample represented aggregates of white to slightly golden curved corrugated scales (sample # 79578, Fig. 1a) from the SNM.
6. Kirovskii apatite mine, Mt. Kukisvumchorr, Khibiny alkaline complex, Kola peninsula, Russia: # Kir4940 from the IVP collection. Hydrotalcite and quintinite forming parallel intergrowths occur in cavities of a calcite veinlet with phlogopite cross-cutting ijolite-urtite. The complex crystals consisting of these hydrotalcite-group minerals are pinkish tablets up to 3 mm across typically combined in rose-like clusters or crusts.

Experimental methods

Chemical composition

The chemical composition of all samples was determined with a scanning electron microscope S3400N (Geomodel Center of St. Petersburg State University) equipped with an AzTec analyzer Energy 350 operating in the energy dispersive spectroscopy (EDS) mode at

20 kV, 1.5 nA and a 5 μm spot size. The standards used for quantification were: MgO (Mg), Al_2O_3 (Al), FeS_2 (Fe), Cr metal (Cr) and Mn metal (Mn). Quinitinite of known chemical composition was also used as a standard. The average chemical data obtained for samples are given in Table 1.

The IR spectra of the hydrotalcite samples were recorded using a Bruker Vertex IR spectrometer (XRD Resource Centre, St. Petersburg State University). The measurements were taken at room temperature using the KBr technique.

The water content was measured for samples 105371 and 10532 by differential scanning calorimetry (DSC) coupled with thermogravimetric analysis (TGA). The experiment was performed using a DSC/TGA Netzsch STA 449 F3 instrument (XRD Resource Centre, St. Petersburg State University), measuring from 30–1200 °C with a ramp rate of 10 °C min^{-1}, gas flow 20 ml min^{-1} by heating the samples under Ar-Ar atmospheres.

Single-crystal X-ray diffraction data

Crystals from samples (i) 9699, Kir4940 and (ii) 10604 were studied at RT, the measurements were carried out by means of a (i) Bruker Kappa Apex Duo (Mo*K*α) diffractometer operated at 45 kV and 0.6 mA (microfocus source) and (ii) Bruker Smart Apex (Mo*Kα*) diffractometer operated at 50 kV and 40 mA (Table 2), respectively (both in XRD Centre, St. Petersburg State University). Another crystal selected from the 9699 specimen and labeled below as 9699 LT and sample 80947 were studied by means of Bruker APEX-II CCD diffractometer (Durham University), the measurements were carried out at T = 120 and 93 K, respectively (Table 2). All instruments are equipped with CCD detectors. The intensity data were reduced and corrected for Lorentz, polarization and background effects using the Bruker software APEX2 (Bruker-AXS, 2014). A semi-empirical absorption-correction based upon the intensities of equivalent reflections was applied (SADABS, Sheldrick, 2015). The unit-cell parameters (Table 2) were refined by the least-squares methods. The Shelxtl program package

was used for the structure solution and refinement (Sheldrick, 2015). Crystal data, parameters of data collection and refinement details are given in Table 2.

Powder X-ray diffraction data

Initially, the homogeneity of all samples was checked by means of a desktop diffractometer Bruker D2 Phaser with a Bragg–Brentano geometry operated at 30 kV/10 mA, and equipped with a LYNXEYE detector (Cu*K*α and Co*K*α). The data collection was carried out under the following conditions: step scan size 0.02°, counting time 1 s, 2θ range is 5–65°. The study revealed a significant preferred orientation of hydrotalcite crystals; however, it allowed for the detection of possible splitting of basal reflections due to the coexistence of visually inseparable phases with different *d*-values.

More thorough powder X-ray diffraction study was done by means of a Rigaku R-AXIS Rapid II single-crystal diffractometer equipped with a cylindrical image plate detector using Debye-Scherrer geometry (*d* = 127.4 mm; Co*K*α). The data were converted using osc2xrd program (Britvin *et al*., 2017).

Results

Chemical composition

All samples contain Mg and Al as species-defining cations, whereas Mn, Fe and Cr are minor observed components. Fe is considered as Fe^{3+} in accord with Mills *et al*. (2016). The empirical formula was calculated on the basis of Mg+Al+Fe+Mn+Cr = 8 *apfu*. The carbonate content was calculated based on charge balance. The amount of OH groups was taken as 2 per 1 cation based on stoichiometry. The H_2O content was measured by DSC and TG analyses and is in agreement with the H_2O content in the ideal chemical formula of hydrotalcite-group minerals (*i.e.*, 0.5 H_2O per 1 cation, see below).

The representative IR spectrum recorded for the sample 10532 is shown in Fig. 2. The spectrum contains the following bands: 3537 (Mg/Al-OH), 3200-2700sh (H_2O interacting with interlayer carbonate), 1655 (H_2O), 1370 (CO_3), 920-910sh (Al-OH), 858 (CO_3 or/and OH), 720-710sh (Al-OH), 664 (Mg-OH), 556 (*M*-O, *M*-O-*M* and O-*M*-O) and 447 (*M*-O, *M*-O-*M* and O-*M*-O) (Hernandez-Moreno *et al.*, 1985; Moroz and Arkhipenko, 1991; Kloprogge *et al.*, 2002; Kloprogge, 2005; Frost *et al.*, 2009).

The DCS and TGA curves (Fig. 3) were interpreted as follows: 1) 30-70 °C loss of absorbed and/or adsorbed water; 2) 70-210 °C loss of interlayer H_2O with corresponding mass loss of 11.8 % that coincides with ideal stoichiometry, i.e. an H_2O molecule per 2 cations; 3) the second strong effect and a mass loss at 365-430 °C is attributed to dehydroxylation and decarbonation of hydrotalcite (Kanezaki, 1998; Frost *et al.*, 2003; Panikorovsky *et al.*, 2015).

Single-crystal X-ray diffraction data

The data obtained for the samples 9699 [at room temperature (RT) and T = 120 K (LT)] and Kir4940 were indexed in the rhombohedral unit cell, space group $R3$ (Table 2). Their diffraction patterns contain only reflections that correspond to the systematic absences condition $-h + k + l = 3n$. The positions of atoms in the metal hydroxide layer were determined in the space group $R3$. The test for a higher symmetry applying the PLATON program (Speck, 2003) indicated the space group $R\bar{3}m$. The hydrogen and interlayer atoms were added to the refinement after structure transformation to the space group $R\bar{3}m$. The diffraction data (Fig. 4) obtained for single crystals from samples 10532, 10604, and 80947 [T = 93 K] were indexed in the hexagonal space group $P6_3/mmc$, unit-cell parameters are given in Table 2. The appearance of weak inconsistent reflections observed in Fig. 4c is due to the single-crystal imperfections. Atom coordinates, site occupancies and displacement parameters are given for 3*R* and 2*H* polytypes in Tables 3 and 4. Selected interatomic distances are provided in Table 5. The

crystallographic information files have been deposited with the Principal Editor of *Mineralogical Magazine* and are available as Supplementary material (see below).

Crystal structures of both rhombohedral and hexagonal hydrotalcite polytypes (Fig. 5) consist of metal hydroxide layers. The long-range average crystal structures as determined by X-ray diffraction contain one *M*1 site statistically occupied by Mg and Al and impurity elements (Fe) with M^{2+}:M^{3+} ~ 3:1 (Table 1). Rhombohedral and hexagonal modifications differ from one another by stacking sequences of metal hydroxide layers, having 3-layer and 2-layer periodicity, respectively (Fig. 5). For both hydrotalcite-3*R* and 2*H*, anisotropic displacement parameters were refined for the O and *M* sites in the octahedral layer; for the rest of the atoms (H of octahedral layer and interlayer C and O atoms) only isotropic displacement parameters were refined. The occupancies of the *M* and O sites in the octahedral layer were determined as close to 100 % in all samples and were fixed at 1.02 for *M*1 (0.75Mg + 0.25Al, refined using scattering curve of Mg) and 1.0 for O in agreement with ideal chemical formula. The position of H atoms in the metal hydroxide layer is fixed by symmetry in the *x* and *y* coordinates (Tables 3, 4) and may vary only along *z*, the O-H distances were restrained at 0.82(2) Å for all samples (Table 5).

Fig. 6 shows the residual electron density maps at the interlayer level. The map contains toroidal rings that refer to the interlayer O atoms with C atoms located in between. In the interlayer, positions of carbonate groups (carbon and oxygen) were determined, whereas positions of H_2O molecules could not be localized. Due to the smearing of electron density, the interlayer species are difficult to refine. For the sample 10604, the C2-O3 distance was softly restrained to be 1.21(5) Å, whereas in other samples reliable C-O distances were obtained without restrains (Table 5). The absence of significant changes between the electron density maps obtained at room and low temperatures (Fig. 6) indicates the statistic nature of disorder of the interlayer atoms.

Powder X-ray diffraction data

Powder X-ray diffraction experiments performed in a Bragg-Brentano geometry reveal splitting of basal reflections (003, 006, 009) for the sample Kir4940 indicating coexistence of two phases: one with d_{003} = 7.76 Å and another with d_{003} = 7.56 Å (Fig. 7). Our previous investigations indicated a characteristic hydrotalcite *d*-value of 7.80 Å and typical quintinite *d* value of 7.56 Å (due to the difference in the M^{2+}:M^{3+} ratio [Zhitova *et al*., 2016]). Therefore, the main phase with d_{003} = 7.76 Å is hydrotalcite, whereas the second phase with d_{003} = 7.56 Å is quintinite. The rest of the samples were considered as having only M^{2+}:M^{3+} ~ 3:1 because they contained one set of basal reflections with *d* ~ 7.80 Å only. The powder X-ray diffraction pattern recorded for Kir4940 by means of the Rigaku R-AXIS Rapid II diffractometer (from smaller sample) exhibits only hydrotalcite reflections, *d* ~ 7.80 Å.

The indexing of the powder X-ray diffraction patterns recorded for seven hydrotalcite samples using randomized material is shown in Fig. 8. As indicated by the reflection positions in Fig. 8a,b, some reflections overlap for the 3*R* and 2*H* polytypes. Characteristic reflections that can be used for separation of 3*R* and 2*H* phases are located in the 2θ range of 40-60 °. The experimentally obtained diffraction patterns (Fig. 8) show the presence of only 3*R* polytype in Kir4940; only 2*H* polytype in 10532 and 10604; the mixture of 3*R* and 2*H* polytypes with the predominance of 3*R* in 158518, 79578, and 52071 and with the predominance of 2*H* in 105371.

Discussion

Hydrotalcite localities and distribution of 3R and 2H polytypes

The present work confirms the unambiguous presence of hydrotalcite in Snarum (3*R* and 2*H*), Zelentsovskaya pit (2*H*), Praskov`e-Evgenievskaya pit (2*H*), Talnakh (3*R*), St. Lawrence (3*R* and 2*H*), and Khibiny (3*R*). Our data on the sample 10532 from the Zelentsovskaya pit are in good agreement with the previous studies of hydrotalcite (formerly “manasseite”) from the same locality by Ivanov and Aizikovich (1980). These authors reported this material to be

hydrotalcite-2*H* with d = 7.77 Å. The crystal chemical characteristics, *i.e.*, polytype identification and d ~ 7.80 Å for hydrotalcite from Snarum obtained in this work coincide with those reported previously by Mumpton *et al*. (1965), Paush *et al*. (1986) and Mills *et al*. (2016). Based on the literature data for hydrotalcite (Frondel, 1941), pyroaurite (Aminoff and Broomé, 1931; Frondel, 1941; Ingram and Taylor, 1967; Allmann, 1968) and stichtite (Mills *et al*., 2011; Zhitova et al., 2019), one can expect intimate intergrowths of 3*R* and 2*H* polytypes for these minerals as the most typical case. However, our data show that hydrotalcite samples represented by pure 3*R* or 2*H* polytype are also common, and the single-polytype samples demonstrate more perfect crystals. Moreover, our study indicates the existence of only "classical" 3*R* and 2*H* polytypes of hydrotalcite, *i.e.*, with no long-range ordering of cations within the octahedral layers or anions in the interlayer that would produce a superstructure detectable by X-ray diffraction.

For hydrotalcite-supergroup members with M^{2+}:M^{3+} = 3:1 and their synthetic analogues, the existence of polytypes comprising doubled and tripled unit-cell parameters (as discussed in the Introduction) in comparison to the "classical" 2*H* and 3*R* polytypes (*i.e.*, a 6*R* polytype) should be rationalized and confirmed by particular crystal chemical reasons such as cation/anion ordering, stacking sequences, mutual arrangement of layer and interlayer species, whereas simple adoption of data from powder diffraction databases may result in the incorrect indexing of powder X-ray diffraction pattern. Thus, correct indexing of powder diffraction patterns and identification of structure for hydrotalcite and isotypic minerals and synthetic compounds requires careful consideration of possible superlattice reflections, peak intensities and their rationalization.

Unit-cell metrics of hydrotalcite and quintinite

It is worth noting that the crystal structures of hydrotalcite-3*R* and quintinite-3*R* are topologically identical, as well as the crystal structures of hydrotalcite-2*H* and quintinite-2*H*. The crystallographic difference between hydrotalcite and quintinite is evidenced in the unit-cell

dimensions. The range of polytypes shown by both hydrotalcite- and quinitine-group minerals means that polytype cannot serve as an indicator of the group to which a mineral belongs. In principle, the compositionally distinct hydrotalcite and quintinite minerals can be distinguished by the dimensions of their subcells, specifically the distance $a`$ between two adjacent cations in the octahedral layer (*M*-*M*), which is equal to the *a* parameter if there is no long-range order in the layers, and the layer spacing $d_{00n}$ of an *n*-layer polytype. The reported values for quintinite are: $a`$ = 3.02–3.06 Å and d ~ 7.56 Å (Allmann and Jepsen, 1969, Arakcheeva *et al*., 1996, Chao and Gault, 1997, Krivovichev *et al*., 2010a,b, Zhitova *et al*., 2010, 2018a,b). The reported values for hydrotalcite are: $a`$ = 3.05-3.07 Å and $d$ ~ 7.80 Å (Mills *et al*., 2016, Zhitova *et al*., 2016 and references therein). Thus, due to the overlap of $a`$ for quintinite and hydrotalcite (that may be even stronger for different compositions) only the *d*-value (neither polytype nor $a`$) can serve as a diagnostic crystallographic feature for distinguishing hydrotalcite from quintinite (Zhitova *et al*., 2016).

Metal hydroxide layer: M^{2+}:M^{3+} ratios and superstructures

Based on the assumption that hydrotalcite-supergroup members with M^{2+}:M^{3+} = 2:1 and 3:1 are more common in nature than samples with other ratios, Hofmeister and von Platen (1992) proposed the presence of a long-range cation ordering within metal hydroxide layers that dictates the ratio preference (Evans and Slade, 2006). The theoretical schemes (Fig. 9) of ordered cation patterns imply, in accord with Hofmeister and von Platen (1992):

(i) 2×2 (hexagonal) or $\sqrt{3} \times 2$ (orthorhombic) superstructure for hydrotalcite;

(ii) $\sqrt{3} \times \sqrt{3}$ in-plane superstructure for quintinite.

Richardson (2013) re-examined the different ways M^{3+} distribution may occur in metal hydroxide layers from a theoretical point of view and validated all three superstructures as crystal-chemically possible. We should note that for the correct understanding of discussion given below we need to distinguish the following types of atomic order and disorder: (i) three-

dimensional long-range order which results in additional (superstructure) Bragg reflections; (ii) two-dimensional long-range order or three-dimensional short-range order, which at best result in extended rods or sheets of diffuse scattering in reciprocal space, but may not result in any diffraction evidences; (iii) true disorder at the unit cell scale.

It is noteworthy that the ordering of M^{2+} and M^{3+} cations according to the $\sqrt{3} \times \sqrt{3}$ superstructure was experimentally registered by single-crystal X-ray diffraction study for numerous samples of hydrotalcite-supergroup minerals with M^{2+}:M^{3+} = 2:1, including quintinite (Table 6). The $\sqrt{3} \times \sqrt{3}$ superstructure was also proved for a number of synthetic LDHs by the detection of superstructure reflections in the powder X-ray diffraction patterns (Sissoko *et al*., 1985; Britto *et al*., 2008; Britto and Kamath, 2009; Marappa and Kamath, 2015). In contrast, neither 2 × 2 nor $\sqrt{3}$ × 2 superstructure have been confirmed for hydrotalcite-supergroup members by single-crystal or powder X-ray diffraction. In the present study, we have found no reflections that could give a hint on the presence of the M^{2+}-M^{3+} ordering. However, the absence of such superstructure reflections cannot uniquely serve as an evidence for the absence of a local superstructure (two-dimensional long-range order or three-dimensional short-range order). This is because the cation ordering within a single metal hydroxide layer may be lost in the third dimension due to the irregular localization (and thus registration) of the M^{3+} cations in adjacent layers (as a result of weak bonding). The quite common alternative explanation that the M^{2+}-M^{3+} ordering cannot be observed due to the similar scattering power of Mg and Al is disproved by the experimental observation of scattering from long-range Mg-Al ordering for three polytypes of quintinite (Table 6). Below we provide a short review of the previous studies of the M^{2+}-M^{3+} ordering for hydrotalcite-group minerals and their synthetic analogues by different techniques.

The experimental evidence of a 2 × 2 superstructure (a ~ 6.2 Å) is an image obtained by scanning tunnel microscopy for synthetic "hydrotalcite" having high Cl content with the chemical formula $[Mg_6Al_2(OH)_{16}](CO_3)_{1/2}Cl(H_2O)_2$ (Yao *et al*., 1998). However, the same

crystal studied by atomic force microscopy was reported as having no obvious superstructure (a ~ 3.1 Å). Different superstructures were observed for the same material during anion-exchange experiments and were interpreted as anion rather than cation ordering (Yao *et al*., 1998). Based on the ion-exchange chromatography on acid digests of stichtite, $[Mg_6Cr^{3+}_2(OH)_{16}](CO_3)(H_2O)_4$, Hansen and Koch (1996) concluded that M^{2+} and M^{3+} distribution is not always completely random (implying local ordering of type (ii)). Drits and Bookin (2001) concluded that hydrotalcite, pyroaurite and desautelsite, $[Mg_6Mn^{3+}_2(OH)_{16}](CO_3)(H_2O)_4$, are characterized by a random distribution of M^{2+} and M^{3+} cations (implying the absence of long-range ordering) by analyzing powder X-ray diffraction patterns and literature data. Multinuclear nuclear magnetic resonance spectroscopy of synthetic Mg-Al LDHs with different M^{2+}:M^{3+} ratios indicated a completely ordered cation distribution in the LDH sample with M^{2+}:M^{3+} = 2:1 (type (i)) and nonrandom distribution of cations for LDHs with higher M^{2+}:M^{3+} ratios (including M^{2+}:M^{3+} = 3:1), with no M^{3+}-M^{3+} close contacts (Sideris *et al*., 2008), i.e. the absence of long-range ordering for M^{2+}:M^{3+} = 3:1. Local ordering of Al^{3+} cations (type (ii)) in synthetic Zn_3Al-I LDHs according to the orthorhombic superstructure was suggested by Aimoz *et al*. (2012) based on extended X-ray absorption fine structure (EXAFS) data. Finally, the early study of pyroaurite (Fe^{3+}-analogue of hydrotalcite) by selected-area electron diffraction (Ingram and Taylor, 1967) indicated no superstructure (a ~ 3. 1 Å), but some areas gave the $\sqrt{3} \times \sqrt{3}$ superstructure that was attributed to differing M^{2+}:M^{3+} ratio. These results on absence on long-range ordering of M^{2+} and M^{3+} cations in pyroarite are in agreement with structure determination done by Allmann and Lohse (1966).

In general, no definite conclusion exists on the distribution of M^{2+}-M^{3+} cations in the LDHs with M^{2+}:M^{3+} = 3:1. The literature data mainly suggest local ordering of M^{2+} and M^{3+} cations within the metal hydroxide layer, in contradiction to the idea of Hofmeister and von Platen (1992). In our study, we found no signs of any superstructure in hydrotalcite that can be observed by X-ray diffraction methods, which does not deny that local ordering of type (ii) (two-

dimensional long-range order or three-dimensional short-range order) occurs. We suggest that the potential insight into this issue of M^{2+} and M^{3+} ordering for LDHs with M^{2+}:M^{3+} = 3:1 can be obtained through the techniques sensitive to the precise positions and orientations of carbonate ions (by comparison of the LDHs with M^{2+}:M^{3+} = 2:1 and 3:1, i.e. by spectroscopic methods), because these characteristics have to reflect the localization of charge-bearing M^{3+} cations. Finally, this seems to be highly crystal-chemically possible that complete disorder (type (iii)) is unlikely, and that local order of type (ii) can be very strong despite there being too little long-range (type (i)) coupling between layers to produce extra Bragg peaks. Thus, diffraction data may not show the true much higher state of local cation order, and can indicate completely random distribution where methods giving information on local structure of the same material may show otherwise. This would explain the apparent contradictions between data obtained using different techniques.

Acknowledgements

We express our gratitude to of Smithsonian National Museum of Natural History (Washington, DC, USA) and Fersman Mineralogical Museum of Russian Academy of Sciences (Moscow, Russia) for collaboration. The experiments were done using facilities of XRD and Geomodel Resource Centers of St. Petersburg State University and at Durham University. An initial visit to Durham University for EZ (2015-2016) was funded by the British Council Research Program. We thank Andrey Batsanov (Durham University) for collecting some of X-ray diffraction data. This study was supported by the Russian Science Foundation (grant 17-77-10023). We thank Peter Leverett and two anonymous reviewers for their suggestions and Associate Editor Anthony Kampf and Principal Editor Stuart Mills for manuscript handling.

Supplementary material

To view supplementary material for this article, please visit https://doi.org/10.1180/mgm.2018.145

Reference

Aimoz, L., Taviot-Guého, C., Churakov, S.V., Chukalina, M., Dähn, M., Curti, E., Bordet, P., and Vespa M. (2012) Anion and Cation Order in Iodide-Bearing Mg/Zn−Al Layered Double Hydroxides. *The Journal of Physical Chemistry*, **116**, 5460−5475.

Allmann, R. (1968) The crystal structure of pyroaurite. *Acta Crystallographica*, **B24**, 972–977.

Allmann, R. (1977) Refinement of the hybrid layer structure $[Ca_2Al(OH)_6]^+$ $[½SO_4 \cdot 3H_2O]^-$. *Neues Jahrbuch für Mineralogie, Monatshefte*, **1977**, 136−144.

Allmann, R. and Jepsen, H.P. (1969) Die struktur des Hydrotalkits. *Neues Jahrbuch für Mineralogie, Monatshefte*, **1969**, 544−551.

Allmann, R. and Lohse, H.-H. (1966) Die Struktur des Hydrotalkits. *Neues Jahrbuch für Mineralogie, Monatshefte*, **1966**, 161-180.

Aminoff, G. and Broomé, B. (1931) Contribution to the knowledge of the mineral pyroaurite. *Kungliga Svenska Vetenskapsakademiens Handlingar*, **9**, 23−48.

Arakcheeva, A.V., Pushcharovskii, D.Yu., Atencio, D. and Lubman, G.U. (1996) Crystal structure and comparative crystal chemistry of $Al_2Mg_4(OH)_{12}(CO_3)\times 3H_2O$, a new mineral from the hydrotalcite- manasseite group. *Crystallography Reports*, **41**, 972−981.

Bellotto, M., Rebours, B., Clause, O., Lynch, J., Bazin, D. and Elkaim, E. (1996) A reexamination of hydrotalcite crystal chemistry. *The Journal of Physical Chemistry*, **100**, 8527–8534.

Bonaccorsi, E., Merlino, S. and Orlandi, P. (2007) Zincalstibite, a new mineral, and cualstibite: Crystal chemical and structural relationships. *American Mineralogist*, **92**, 198−203.

Britto, S. and Kamath, P.V. (2009) Structure of bayerite-based lithium−aluminum layered double hydroxides (LDHs): observation of monoclinic symmetry. *Inorganic Chemistry*, **48**, 11646-11654.

433 Britto, S., Thomas, G.S., Kamath, P.V. and Kannan, S. (2008) Polymorphism and structural
434 disorder in the carbonate containing Layered Double Hydroxides of Al and Li. *The Journal*
435 *of Physical Chemistry*, **C112**, 9510-9515.
436 Britvin, S.N., Dolivo-Dobrovolsky, D.V. and Krzhizhanovskaya, M.G. (2017) Software for
437 proceedings the X-ray powder diffraction data obtained from the curved image plate
438 detector of Rigaku RAXIS Rapid II diffractometer. *Zapiski Rossiiskogo*
439 *Mineralogicheskogo Obshchestva*, **146**, 104-107 (in Russian).
440 Bruker-AXS (2014) APEX2. Version 2014.11-0. Madison, Wisconsin, USA.
441 Chao, G.Y. and Gault, R.A. (1997) Quintinite-2*H*, quintinite-3*T*, charmarite-2*H*, charmarite-3*T*
442 and caresite-3*T*, a new group of carbonate minerals related to the hydrotalcite/manasseite
443 group. *The Canadian Mineralogist*, **35**, 1541−1549.
444 Cocheci, L., Barvinschi, P., Pode, R., Popovici, E. and Seftel, E.M. (2010) Structural
445 characterization of some Mg/Zn-Al type hydrotalcites prepared for chromate sorption
446 from wastewater. *Chemical Bulletin of "Politehnica" of Timisoara, Romania*, **55**, 40−45.
447 Cooper, M.A. and Hawthorne, F.C. (1996) The crystal structure of shigaite,
448 $[AlMn_2(OH)_6]_3(SO_4)_2\ Na(H_2O)_6\{H_2O\}_6$, a hydrotalcite-group mineral. *The Canadian*
449 *Mineralogist*, **34**, 91−97.
450 Drits, V.A. and Bookin, A.S. (2001) Crystal structure and X-ray identification of layered double
451 hydroxides. In: Rives (2001), 39−92.
452 Evans, D.G. and Slade, R.C.T. (2006) Structural aspects of layered double hydroxides. Layered
453 Double Hydroxides (Duan X. and Evans D.G., editors). Springer, Berlin, **119**, 1−87.
454 Frondel, C. (1941) Constitution and polymorphism of the pyroaurite and sjögrenite groups.
455 *American Mineralogist*, **26**, 295−315.
456 Frost, R.L., Martens W., Ding Z. and Kloprogge J.T. (2003) DSC and high-resolution TG of
457 synthesized hydrotalcites of Mg and Zn. *Journal of Thermal Analysis and Calorimetry*,
458 **71**, 429-438.

459 Frost, R.L., Spratt, H.J. and Palmer, S.L. (2009) Infrared and near-infrared spectroscopic study
460 of synthetic hydrotalcites with variable divalent/trivalent cationic ratios. *Spectrochimica*
461 *Acta A*, **72**, 984−988.
462 Hansen, H.C.B. and Koch, C.B. (1996) Local ordering of chromium(III) in trioctahedral
463 hydroxide sheets of stichtite studied by ion exchange chromatography. *Clay Minerals*, **31**,
464 53−61.
465 Hernandez-Moreno, M.J., Ulibarri, M.A., Rendon, J.L. and Serna, C.J. (1985) IR characteristics
466 of hydrotalcite-like compounds. *Physics and Chemistry of Minerals*, **12**, 34−38.
467 Hochstetter, C. (1842) Untersuchung über die zusammensetzung einiger mineralien. *Journal für*
468 *Praktische Chemie*, **27**, 375−378.
469 Hofmeister, W. and Von Platen H. (1992) Crystal Chemistry and Atomic Order in Brucite-
470 related Double-layer Structures. *Crystallography Reviews*, **3**, 3−26.
471 Huminicki, D.M.C. and Hawthorne, F.C. (2003) The crystal structure of nikischerite,
472 $NaFeAl_3(SO_4)_2(OH)_{18}(H_2O)_{12}$, a mineral of the shigaite group. *The Canadian Mineralogist*,
473 **41**, 79−82.
474 Ingram, L. and Taylor, H.F.W. (1967) The crystal structures of sjögrenite and pyroaurite.
475 *Mineralogical Magazine*, **36**, 465−479.
476 Ivanov, O.K. and Aizikovich, A.N. (1980) Manasseite from Kusinskoe deposit. *Zapiski*
477 *Rossiiskogo Mineralogicheskogo Obshchestva*, **109**, 479−483 (in Russian).
478 Kanezaki, E. (1998). Effect of atomic ratio Mg/Al in layers of Mg and Al Layered double
479 hydroxide on thermal stability of hydrotalcite-like layered structure by means of in situ
480 high temperature powder X-ray diffraction. *Materials Research Bulletin*, **33**, 773–778.
481 Kloprogge, J.T., Wharton, D., Hickey, L. and Frost, R.L. (2002) Infrared and Raman study of
482 interlayer anions CO_3^{2-}, NO_3^-, SO_4^{2-} and ClO_4^- in Mg/Al-hydrotalcite. *American*
483 *Mineralogist*, **87**, 623−629.
484 Kloprogge, J.T. (ed.). (2005) The application of vibrational spectroscopy to clay minerals and
485 layered double hydroxides. CMS workshop lectures, the Clay Minerals Society, Aurora,
486 Colorado, USA, 285 pp.

Kolitsch, U., Giester, G. and Pippinger, T. (2013) The crystal structure of cualstibite-1*M* (formerly cyanophyllite), its revised chemical formula and its relation to cualstibite-1*T*. *Mineralogy and Petrology*, **107**, 171−178.

Krivovichev, S.V., Yakovenchuk, V.N., Zhitova, E.S., Zolotarev, A.A., Pakhomovsky, Y.A. and Ivanyuk, G.Y., 2010a. Crystal chemistry of natural layered double hydroxides. 1. Quintinite-2*H*-3*c* from the Kovdor alkaline massif, Kola peninsula, Russia. *Mineralogical Magazine*, **74**, 821−832.

Krivovichev, S.V., Yakovenchuk, V.N., Zhitova, E.S., Zolotarev, A.A., Pakhomovsky, Y.A. and Ivanyuk, G.Yu., 2010b. Crystal chemistry of natural layered double hydroxides. 2. Quintinite-1*M*: First evidence of a monoclinic polytype in M^{2+}-M^{3+} layered double hydroxides. *Mineralogical Magazine*, **74**, 833−840.

Krivovichev, S.V., Antonov, A.A., Zhitova, E.S., Zolotarev, A.A., Krivovichev, V.G. and Yakovenchuk, V.N. (2012) Quintinite-1*M* from Bazhenovskoe deposit (Middle Ural, Russia): crystal structure and properties. *Bulletin of Saint-Petersburg State University*, *Ser. Geology and Geography*, **7**, 3−9 (in Russian).

Liao, L., Zhao, N. and Xia, Z. (2012) Hydrothermal synthesis of Mg–Al layered double hydroxides (LDHs) from natural brucite and $Al(OH)_3$. *Materials Research Bulletin*, **47**, 3897–3901.

Marappa, S. and Kamath, P.V. (2015) Structure of the carbonate-intercalated Layered Double Hydroxides: A reappraisal. *Industrial and Engineering Chemistry Research*, **54(44)**, 11075–11079.

Mills, S.J., Whitfield, P.S., Wilson, S.A., Woodhouse, J.N., Dipple, G.M., Raudsepp, M. and Francis, C.A. (2011) The crystal structure of stichtite, re-examination of barbertonite, and the nature of polytypism in MgCr hydrotalcites. *American Mineralogist*, **96**, 179−187.

Mills, S.J., Christy, A.G., Génin, J-M.R., Kameda, T. and Colombo, F. (2012a) Nomenclature of the hydrotalcite supergroup: natural layered double hydroxides. *Mineralogical Magazine*, **76**, 1289−1336.

Mills, S.J., Christy, A.G., Kampf, A.R., Housley, R.M., Favreau, G., Boulliard, J–C. and Bourgoin, V. (2012b) Zincalstibite-9*R*: the first nine-layer polytype with the layered double hydroxide structure-type. *Mineralogical Magazine*, **76**, 1337−1345.

Mills, S.J., Kampf, A.R., Housley, R.M., Favreau, G., Pasero, M., Biagioni, C., Merlino, S., Berbain, C. and Orlandi, P. (2012c) Omsite, $(Ni,Cu)_2Fe^{3+}(OH)_6[Sb(OH)_6]$, a new member of the cualstibite group from Oms, France. *Mineralogical Magazine*, **76**, 1347−1354.

Mills, S.J., Christy, A.G. and Schmitt, R.T. (2016) The creation of neotypes for hydrotalcite. *Mineralogical Magazine*, **80**, 1023−1029.

Moroz, T.N. and Arkhipenko, D.K. (1991) The crystal chemical study of natural hydrotalcites. *Soviet Geology and Geophysics*, **2**, 52-58.

Mumpton, F.A., Jaffe, H.W. and Thompson, C.S. (1965) Coalingite, a new mineral from the New Idria serpentinite, Fresno and San Benito Counties, California. *American Mineralogist*, **50**, 1893−1913.

Panikorovskii, T.L., Zhitova, E.S., Krivovichev, S.V., Zolotarev, A.A., Britivn, S.N., Yakovenchuk, V.N., Krzhizhanovskaya, M.G. (2015) Thermal «memory effect» in quintinite polytypes-2*H*, -3*R*, and -1*M*. *Zapiski Rossiiskogo Mineralogicheskogo Obshchestva*, **144**, 109–119 (in Russian).

Paush, I., Lohse, H.-H., Schurmann, K. and Allmann, R. (1986) Synthesis of disordered and Al-rich hydrotalcite-like compounds. *Clays and Clay Minerals*, **34**, 507−510.

Richardson, I.G. (2013) Classification of possible ordered distributions of trivalent cations in layered double hydroxides and an explanation for the observed variation in the lower solid-solution limit. *Acta Crystallographica*, **B69**, 629−633.

536 Sacerdoti, M. and Passaglia, E. (1988) Hydrocalumite from Latium, Italy: its crystal structure
537 and relationship with related synthetic phases. *Neues Jahrbuch für Mineralogie,*
538 *Monatshefte,* **1988**, 462−475.
539 Sharma, U., Tyagi, B. and Jasra, R.V. (2008) Synthesis and characterization of Mg-Al-CO_3
540 Layered Double Hydroxides for CO_2 absorption. *Industrial and Engineering Chemistry*
541 *Research*, **47**, 9588−9595.
542 Sheldrick, G.M. (2015) Crystal structure refinement with SHELXL. *Acta Crystallographica*,
543 **A71**, 3–8.
544 Sideris, P.J., Nielsen, U.G., Gan, Z. and Grey, C.P. (2008) Mg/Al ordering in layered double
545 hydroxides revealed by multinuclear NMR spectroscopy. *Science*, **321**, 113−117.
546 Sissoko, I., Iyagba, E.T., Sahai, R., and Biloen, P. (1985) Anion intercalation and exchange in
547 $Al(OH)_3$-derived compounds. *Journal of Solid State Chemistry*, **60**, 283-288.
548 Speck, A. (2003) Single-crystal structure validation with the program *PLATON*. *Journal of*
549 *Applied Crystallography,* **36**, 7−13.
550 Stanimirova, T. (2001) Hydrotalcite polytypes from Snarum, Norway. *Annual of the University*
551 *of Sofia, Faculty of Geology*, **94**, 73−80.
552 Taylor, H.F.W. (1973) Crystal structures of some double hydroxide minerals. *Mineralogical*
553 *Magazine*, **39**, 377−389.
554 Walenta, K. (1984) Cualstibite, a new secondary mineral from the Clara Mine in the Central
555 Black Forest (FRG). *Chemie der Erde*, **43**, 255−260 (in German).
556 Wang, X., Bai, Z., Zhao, D., Chai, Y., Guo, M. and Zhang, J. (2013) New synthetic route to Mg-
557 Al-CO_3 layered double hydroxides using magnesite. *Materials Research Bulletin*, **48**,
558 1228−1232.
559 Yao, K., Taniguchi, M., Nakata, M., Takahashi, M. and Yamagishi, A. (1998) Nanoscale
560 imaging of molecular adsorption of metal complex on the surface of a hydrotalcite
561 crystal. *Langmuir*, **14**, 2410−2414.

562 Zhitova, E.S., Yakovenchuk, V.N., Krivovichev, S.V., Zolotarev, A.A., Pakhomovsky, Y.A. and
563 Ivanyuk, G.Y. (2010) Crystal chemistry of natural layered double hydroxides. 3. The
564 crystal structure of Mg, Al-disordered quintinite-2*H*. *Mineralogical Magazine*, **74**,
565 841−848.
566 Zhitova, E.S., Krivovichev, S.V., Pekov, I.V., Yakovenchuk, V.N. and Pakhomovsky, Ya.A.
567 (2016) Correlation between the *d*-value and the M^{2+}:M^{3+} cation ratio in Mg–Al–CO_3 layered
568 double hydroxides. *Applied Clay Science*, **130**, 2−11.
569 Zhitova, E.S., Krivovichev, S.V., Yakovenchuk, V.N., Ivanyuk, G.Yu., Pakhomovsky, Ya.A.
570 and Mikhailova, J.A. (2018a) Crystal chemistry of natural layered double hydroxides. 4.
571 Crystal structures and evolution of structural complexity of quintinite polytypes from the
572 Kovdor alkaline massif, Kola peninsula, Russia. *Mineralogical Magazine*, doi:
573 10.1180/minmag.2017.081.046.
574 Zhitova, E.S., Popov, M.P., Krivovichev, S.V., Zaitsev, A.N. and Vlasenko, N.S. (2018b)
575 Quintinite-1*M* from the Mariinskoe deposit, Ural Emerald Mines, Central Urals, Russia.
576 *Geology of Ore Deposits*, **59(8)**, 745-751.
577 Zhitova E.S., Pekov I.V., Chukanov N.V., Yapaskurt V.O., Bocharov V.N. (2019) Minerals of
578 the stichtite – pyroaurite – iowaite – woodallite system from serpentinites of Terektinsky
579 range, Altay Mountains, Russia. *Russian Geology and Geophysics*, in press.
580
581
582
583
584
585
586
587

588 Figure captions

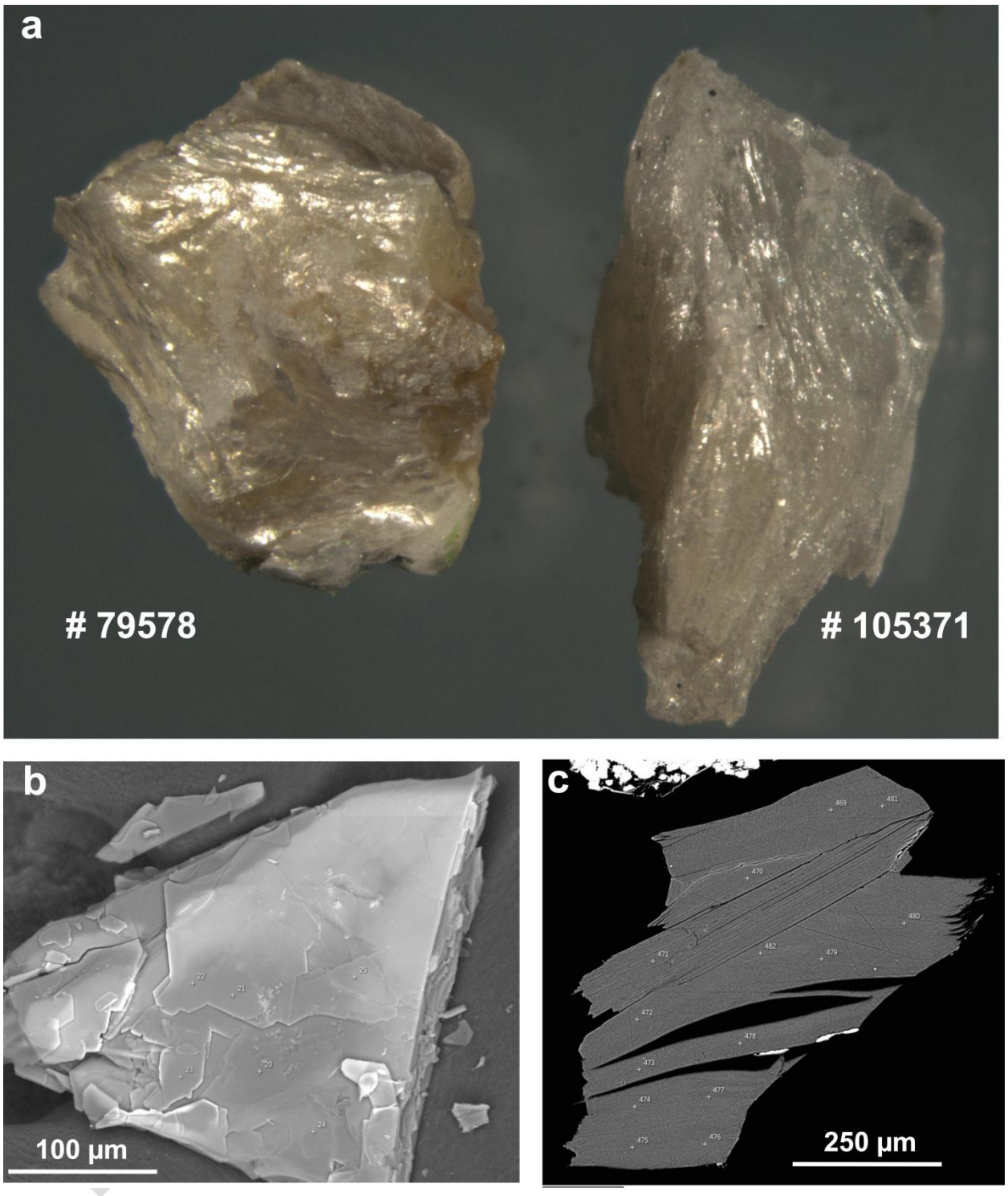

589

590 **FIG. 1**. Images of hydrotalcite samples: (a) photo, (b) BSE image of unpolished grain, sample #
591 9699 and (c) BSE image of polished grain, sample # 10532.

592

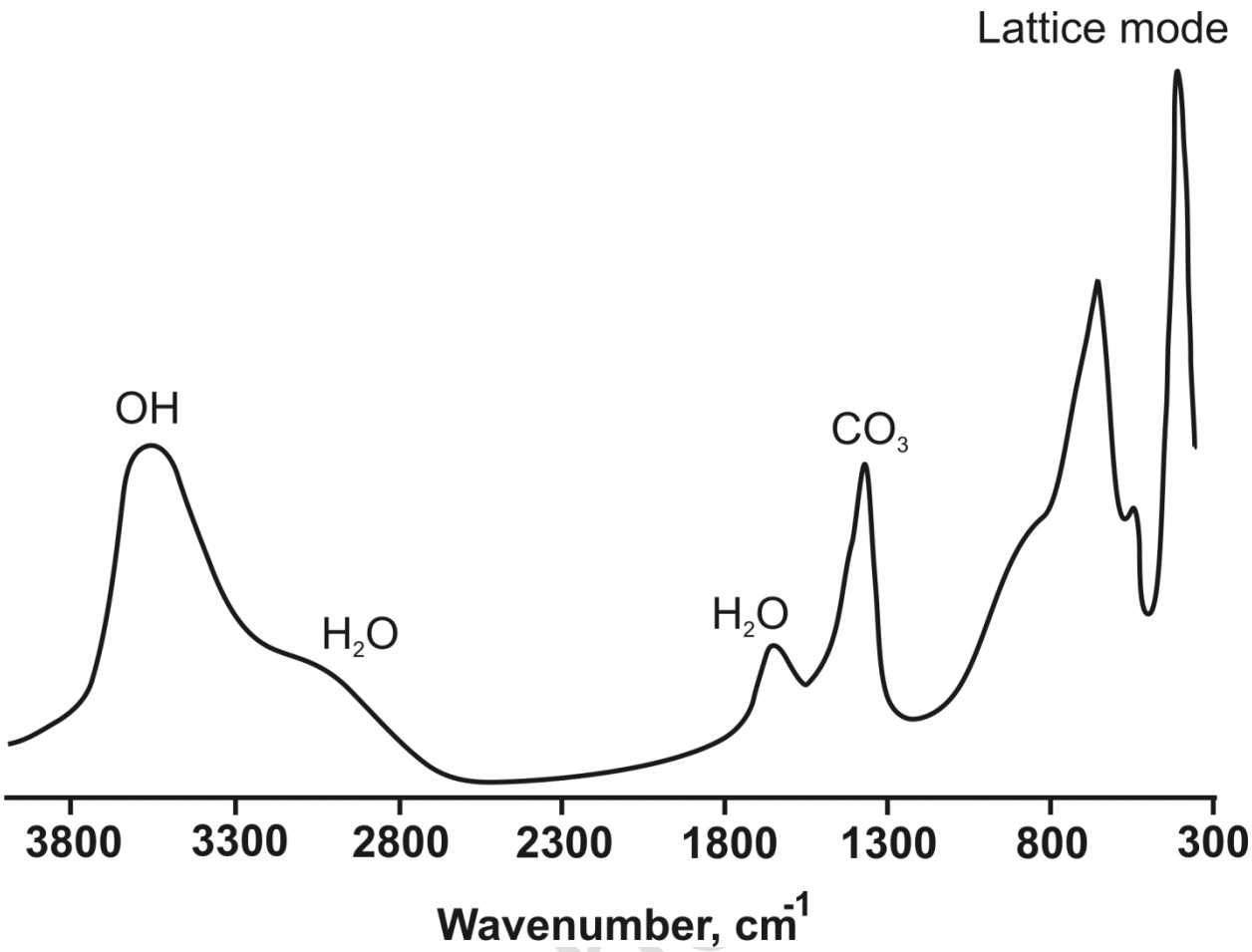

593

594 **FIG. 2**. The infrared spectrum of hydrotalcite, sample 10532.

595

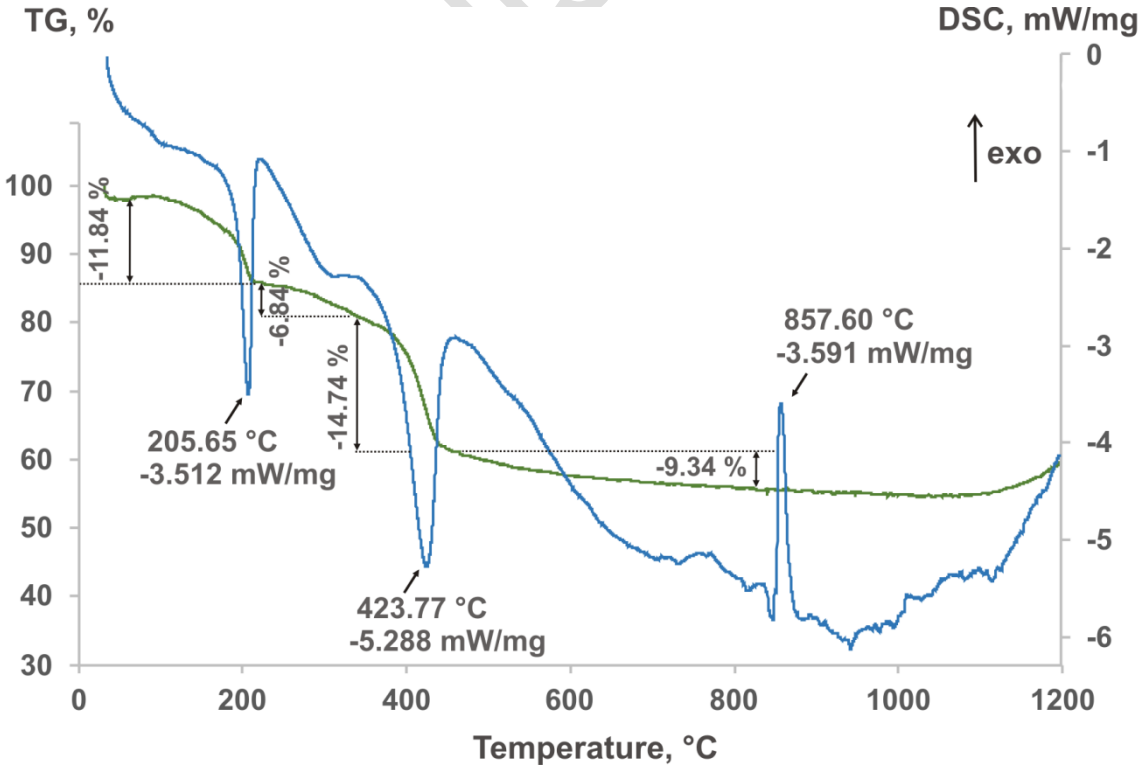

596

597 **FIG. 3**. DCS (blue) and TGA (green) curves of hydrotalcite, sample 105371.

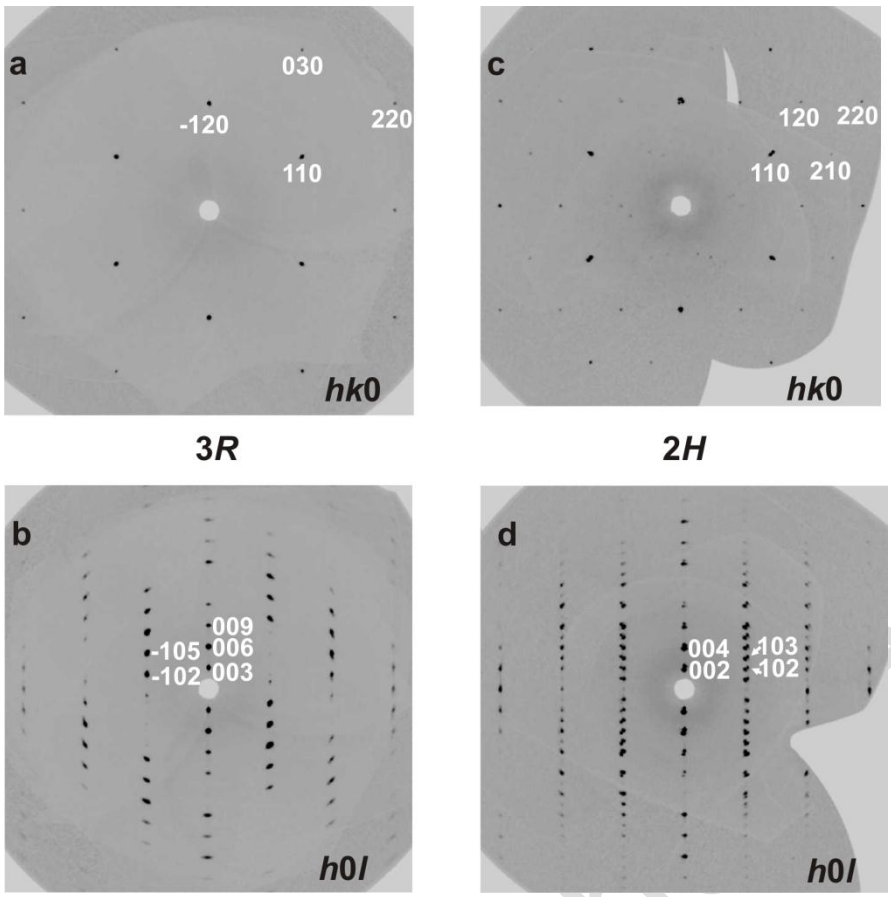

FIG. 4. The *hk*0 (a) and *h*0*l* (b) sections of reciprocal diffraction space obtained for hydrotalcite-3*R* (left) and hydrotaclite-2*H* (right).

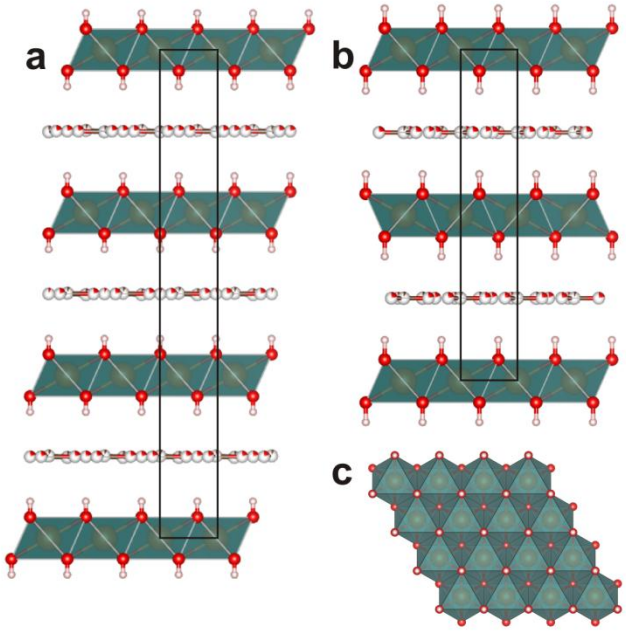

FIG. 5. Crystal structures of 3*R* (a) and 2*H* (b) hydrotalcite polytypes along stacking and (110) projection of metal hydroxide layer (c).

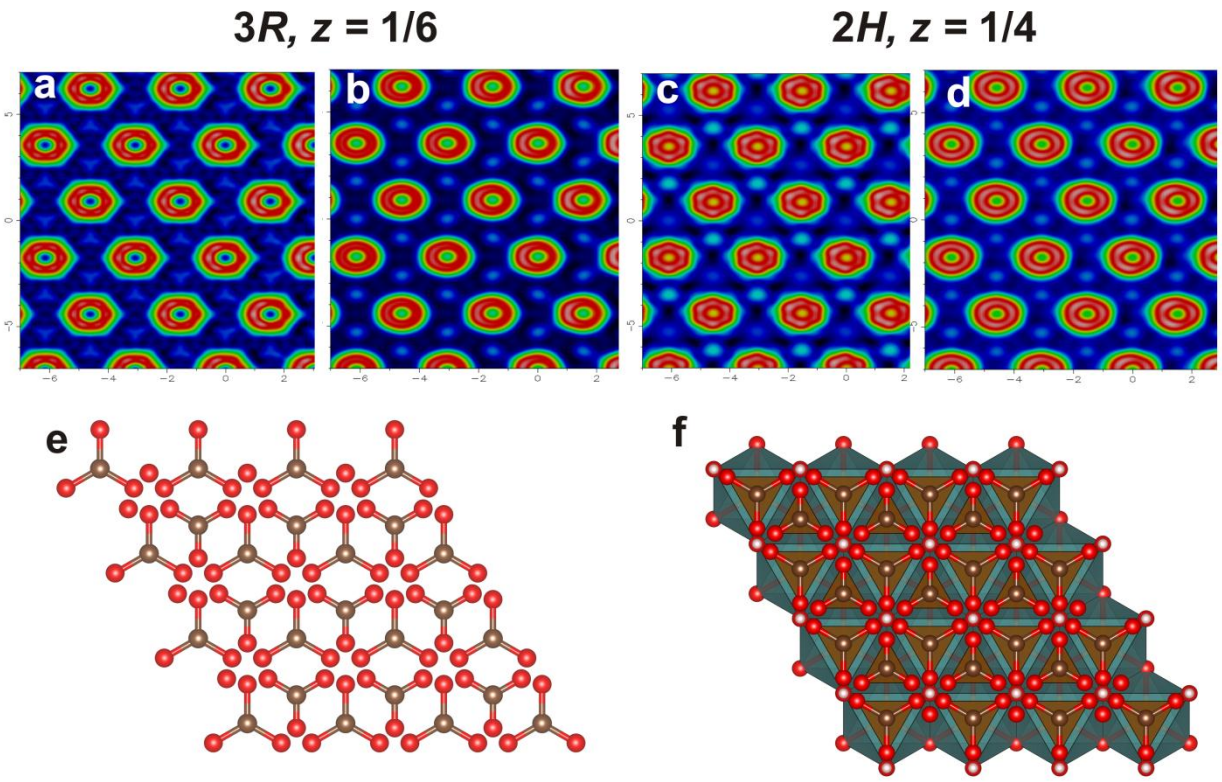

605
606
607 **FIG. 6**. The electron-density maps at the interlayer level: hydrotalcite-3*R* at room temperature
608 (a) and at 120 K (b); hydrotalcite-2*H* at room temperature (c), and at 93 K (d) and topology of
609 interlayer (e) and mutual arrangement of octahedral layer and interlayer (f).
610

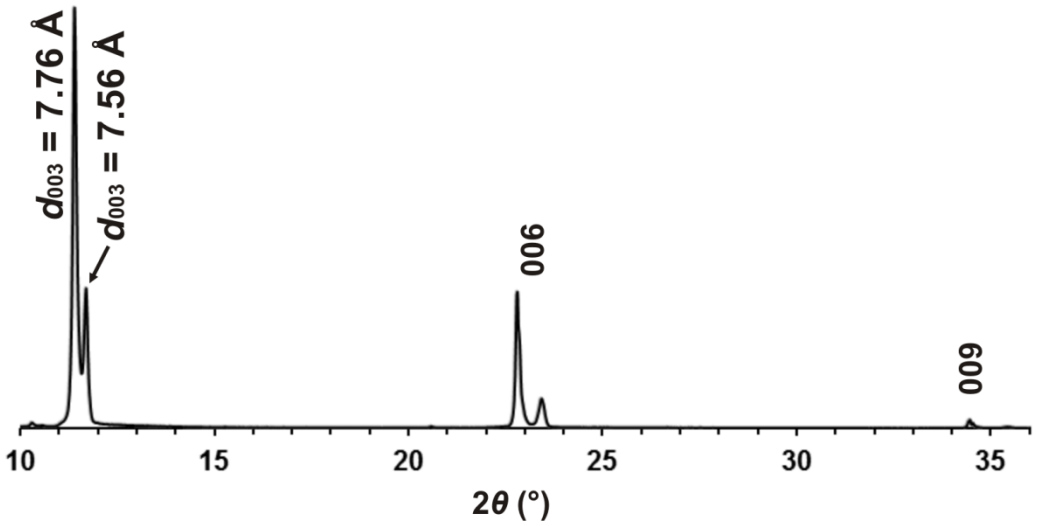

611
612 **FIG. 7**. Powder X-ray diffraction patterns of sample Kir4940 (Cu*K*α), Bragg–Brentano
613 geometry: coexistence of hydrotalcite (d_{003} = 7.76 Å) and quintinite (d_{003} = 7.56 Å).

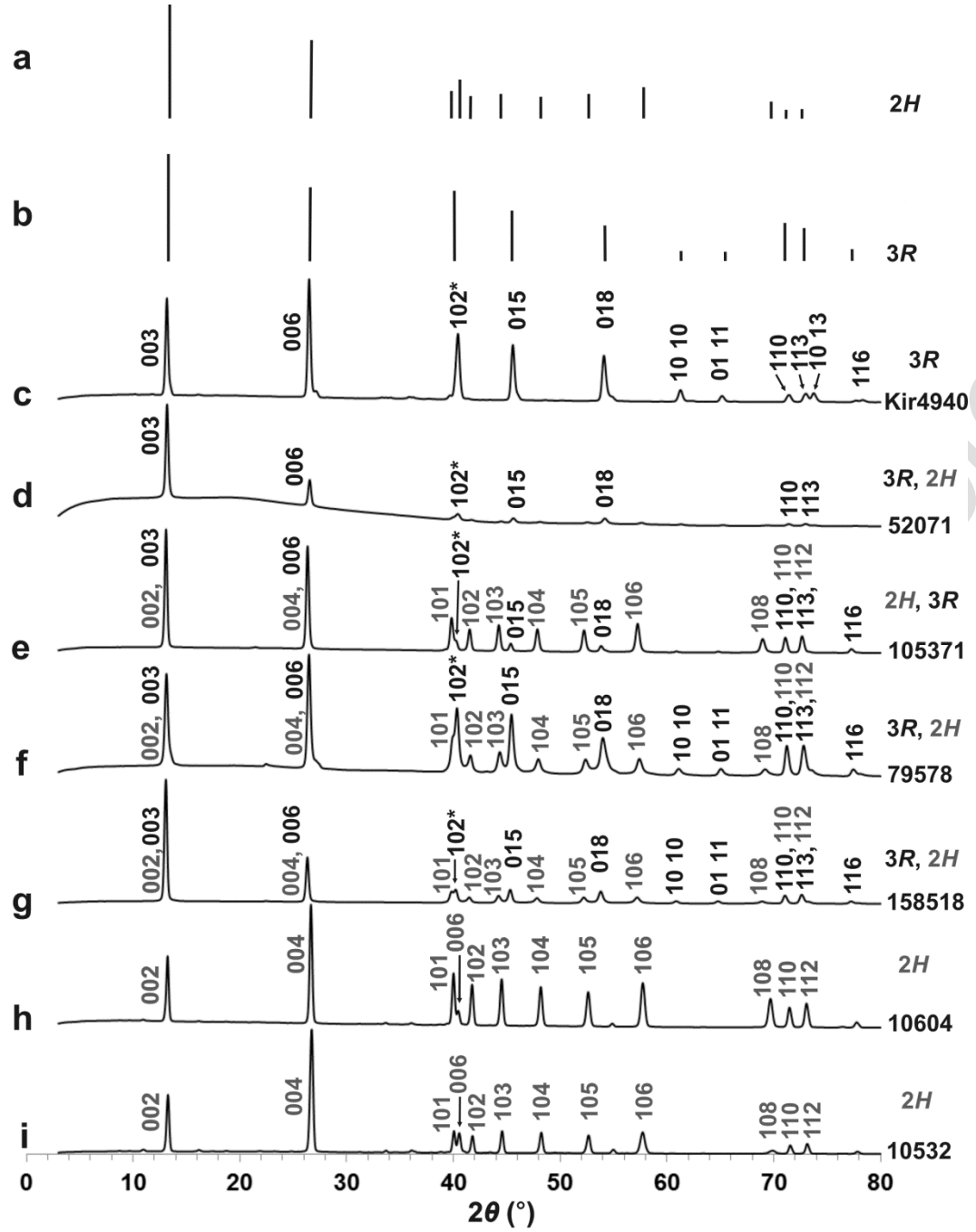

FIG. 8. Powder X-ray diffraction patterns of hydrotalcites (Co*K*α): (a) –reflections for 2*H* polytype; (b) - reflections for 3*R* polytype; (c), (d), (e), (f), (g), (h), (i) – experimental diffractograms, sample numbers are shown on the right side. Reflections of 3*R* and 2*H* are marked as black and gray, respectively. Reflections of 2*H* are observed but not marked for (d) due to very low intensity.

* - 102 reflection of 3*R* is in fact an overlap of 009 and 102, when 2*H* is presented this also overlap with 006.

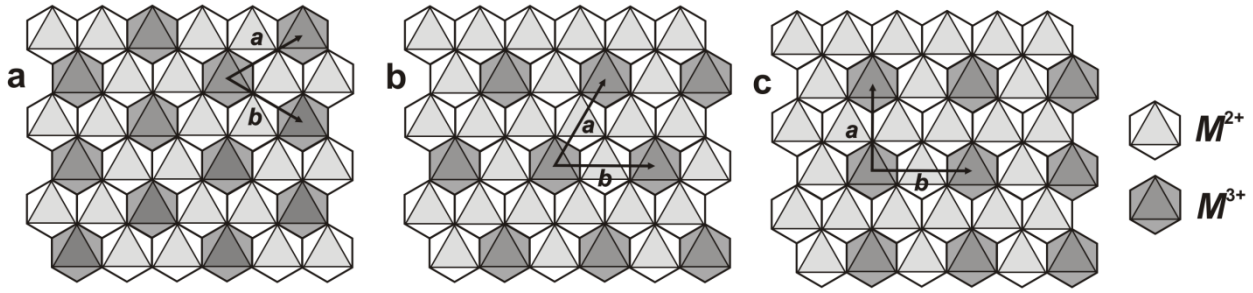

FIG. 9. The (110) projection of metal hydroxide layer: (a) $\sqrt{3} \times \sqrt{3}$ superstructure in quintinite (M^{2+}:M^{3+} = 2:1); (b) theoretical 2 × 2 superstructure in hydrotalcite (M^{2+}:M^{3+} = 3:1) and (c) theoretical $\sqrt{3} \times 2$ superstructure in hydrotalcite (M^{2+}:M^{3+} = 3:1).

Table 1. Chemical composition of hydrotalcite[1]

	52071	105371	158518	10604	10532	80947	9699[2]	79578
wt. %								
MgO	40.04	39.15	37.99	38.41	37.75	38.60	36.10	39.62
MnO	n.d.	0.01	n.d.	n.d.	n.d.	n.d.	n.d.	n.d.
Al_2O_3	15.90	15.23	11.50	17.40	16.00	17.57	14.16	15.41
Fe_2O_3	1.08	1.64	6.61	0.32	1.07	n.d.	3.68	1.19
Cr_2O_3	n.d.	n.d.	n.d.	n.d.	n.d.	0.05	n.d.	n.d.
CO_2[2]	7.20	7.02	6.82	7.60	7.25	7.50	7.12	6.98
H_2O[3]	35.64	34.88	34.20	35.09	34.17	35.21	32.98	35.10
Σ	**99.86**	**97.93**	**97.12**	**98.82**	**96.24**	**98.93**	**94.04**	**98.30**
Formula calculated on the basis of Mg + Mn + Al + Fe^{3+} + Cr^{3+} = 8								
Mg	6.03	6.02	6.03	5.87	5.93	5.88	5.88	6.05
Mn	-	0.00	-	-	-	-	-	-
M^{2+}	**6.03**	**6.02**	**6.03**	**5.87**	**5.93**	**5.88**	**5.88**	**6.05**
Al	1.89	1.85	1.44	2.10	1.99	2.12	1.82	1.86
Fe^{3+}	0.08	0.13	0.53	0.02	0.08	-	0.30	0.09
Cr	-	-	-	-	-	0.00	-	-
M^{3+}	**1.97**	**1.98**	**1.97**	**2.12**	**2.07**	**2.12**	**2.12**	**1.95**
$R = M^{2+}:M^{3+}$	**3.05**	**3.0**	**3.1**	**2.8**	**2.9**	**2.8**	**2.8**	**3.1**
Mg/(Mg+Al+Fe)	0.75	0.75	0.75	0.73	0.74	-	0.73	0.76
Fe/(Al+Fe)	0.04	0.06	0.27	0.01	0.04	-	0.14	0.05
CO_2[3]	0.99	0.99	0.99	1.06	1.04	1.05	1.06	0.98
OH[4]	16	16	16	16	16	16	16	16
H_2O[4]	4	4	4	4	4	4	4	4

[1] chemical composition of sample Kir4940 cannot be provided because it is an intergrowth of quintinite and hydrotalcite
[2] unpolished carbon-coated cleavage surface (Fig. 1);
[3] calculated by charge balance;
[4] calculated by stoichiometry,
n.d. – not determined

Table 2. Crystal data, data collection information and structure refinement details for hydrotalcite

	9699	9699 LT	Kir4940	10604	80947 LT
	Crystal chemical data				
Ideal formula	$[Mg_6Al_2(OH)_{16}][(CO_3)(H_2O)_4]$				
Crystal system	Trigonal			Hexagonal	
Space group	*R*-3*m*	*R*-3*m*	*R*-3*m*	$P6_3/mmc$	$P6_3/mmc$
a, (Å)	3.0728(9)	3.0617(4)	3.0626(3)	3.046(1)	3.0521(9)
c, (Å)	23.326(9)	23.203(3)	23.313(3)	15.477(6)	15.439(4)
d, (Å)	7.76	7.73	7.77	7.74	7.72
Unit-cell volume ($Å^3$)	190.7(1)	188.36(4)	189.37(4)	124.39(8)	124.55(8)
Z	3	3	3	1	1
Calculated density (g/cm^3)	1.92881	1.95235	1.9423	1.9712.065	2.1421.969
Absorption coefficient	0.4117	0.4164	0.41437	0.4209	0.41933
	Data collection				
Diffractometer	Bruker Smart Apex	Bruker ApexPEX-II CCD	Bruker Smart Apex	Bruker Kappa Apex Duo	Bruker APEX-II CCD
Temperature (K)	296	120	296	296	93
Radiation, wavelengths (Å)	Mo-*K*α, 0.71073	Mo-*K*α, 0.71073	Mo-*K*α, 0.71073	Mo-*K*α, 0.71073	Mo-*K*α, 0.71073
θ range (°)	2.62- 50.31	2.63-30.38	2.62- 36.23	1.32- 36.84	2.64-35.19
h, *k*, *l* ranges	-4→5, ±6, -49→47	±4, ±4, ±33	±5, ±5, -37→35	±4, ±5, -25→26	±4, ±4, ±24
Total reflections collected	1366	1057	1066	2792	1326
Unique reflections (R_{int})	304 (0.0581)	101 (0.027)	150 (0.022)	160 (0.027)	142 (0.040)
Unique reflections $F > 2\sigma(F)$	219	99	141	150	126
Data completeness, %	97.4	100	99.3	99.4	100
	Structure refinement				
Refinement method	Full-matrix least-squares on F^2				
Weighting coefficients *a*, *b**	0.120000, 0.1000000.120000, 0.100000	0.089000, 0.8000000.055000, 0.700000	0.130000, 0.0600000.070000, 0.100000	0.120000, 1.2500000.025000, 1.100000	0.120000, 0.8700000.100000, 0.870000
Extinction coefficient	0.0556970.016400	0.1079180.020771	0.0745040	0.1761220	0.1999670.016601
Data/ restrains/ parameters	304/1/13304/0/16	101/10/137	150/10/138	160/2/17	142/1/159
R_1 [$F > 4\sigma(F)$], wR_2 [$F > 4\sigma(F)$]	0.0749, 0.17910.0711, 0.1707	0.03780.0287, 0.12440.0820	0.0292413, 0.16860883	0.0767664, 0.24450701	0.05860.0493, 0.19870.1650
R_1 all, wR_2 all	0.1126, 0.20680.1091, 0.1991	0.03860.0294, 0.12490.0823	0.0423305, 0.16950895	0.08051504, 0.24731521	0.06690.0576, 0.20330.1699
Goodness-of-fit on F^2	1.0681.036	1.0641.019	1.190024	1.084105	1.0360.981
Largest diff. peak and hole ($e Å^{-3}$)	1.29, -0.651.27, -0.55	0.9156, -0.225	0.6853, -0.4623	1.110.87, -1.6072	0.4258, -0.5061

Table 3. Atom coordinates, site occupancies, equivalent isotropic displacement parameters for all atoms and anisotropic displacement parameters for atoms in octahedral layer ($Å^2$) for hydrotalcite-3*R*

Atom	Crystal	Wyckoff position	*x*	*y*	*z*	Occupancy	U_{eq}
				Octahedral layer			
*M*1	9699		0	0	0		0.0106(4)0.0105(4)
	9699 LT	3a	0	0	0	$Mg_{3/4}Al_{1/4}$	0.00610.0047(6)(8)
	Kir4940		0	0	0		0.013118(63)
O1	9699		1/3	2/3	0.0431(1)0.04313(9)	1	0.0189(4)0.0176(5)
	9699 LT	6c	1/3	2/3	0.0433(1)0.04325(9)	1	0.0143(9)0.0119(8)
	Kir4940		1/3	2/3	0.042960(58)	1	0.019685(64)
H1	9699		1/3	2/3	0.0781(8)0.077(3)	1	0.04(2)0.04(2)
	9699 LT	6c	1/3	2/3	0.0785(9)0.079(2)	1	0.03(2)0.03(1)
	Kir4940		1/3	2/3	0.07815(93)	1	0.0710(2)
				Interlayer			
C1	9699		0	0	0.165(2)0.164(2)	0.0625*0.062*	0.020(8)0.020(6)
	9699 LT	6c	0	0	0.166(2)	0.0625*	0.0107(9)
	Kir4940		0	0	0.1678(1)	0.0625*(1)	0.0115(57)
O2	9699		0.138(4)0.130(6)	2/3	1/6	0.0625*0.18(1)	0.040(3)0.049(5)
	9699 LT	18g	0.13829(54)	2/3	1/6	0.178(9)0.0625*	0.0218(3)
	Kir4940		0.14337(34)	2/3	1/6	0.0625*19(1)	0.03546(23)
O3	9699		1/3	2/3	1/6	0.02(4)	0.05*
	9699 LT	3b	1/3	2/3	1/6	0.03(4)	0.00(6)
	Kir4940		1/3	2/3	1/6	0.06(5)	0.1*

Anisotropic displacement parameters of atoms in octahedral layer

Atom	Crystal	U_{11}	U_{22}	U_{33}	U_{23}	U_{13}	U_{12}
*M*1	9699 RT	0.0057(4)0.0056(4)	= U_{11}	0.0203(7)0.0204(8)	0	0	0.0029(2)0.0028(2)
	9699 LT	0.0038(8) 0.0024(6)	= U_{11}	0.012(1)0.0093(8)	0	0	0.0019(4)0.0012(3)
	Kir4940	0.008876(64)	= U_{11}	0.021502(58)	0	0	0.004438(23)
O1	9699 RT	0.0187(6)0.0176(6)	= U_{11}	0.0192(9)0.018(1)	0	0	0.0189(4)0.0088(3)
	9699 LT	0.016(1)0.0134(9)	= U_{11}	0.012(1)0.009(1)	0	0	0.0143(9)0.0067(4)
	Kir4940	0.0202191(85)	= U_{11}	0.018374(97)	0	0	0.0101096(24)

* fixed during refinement

Table 4. Atom coordinates, site occupancies, equivalent isotropic displacement parameters for all atoms (Å^2) and anisotropic displacement parameters for atoms in octahedral layer for hydrotalcite-2*H*

Atom	Crystal	Wyckoff position	*x*	*y*	*z*	Occupancy	U_{eq}
Octahedral layer							
*M*1	10604	2a	0	0	0	$Mg_{3/4}Al_{1/4}$	0.0107094(96)
	80947		0	0	0	$Mg_{3/4}Al_{1/4}$	0.005467(78)
O1	10604	4f	1/3	2/3	0.06434(23)	1	0.0150(18)
	80947		1/3	2/3	0.06489(2)	1	0.01192(1)
H1	10604	4f	1/3	2/3	0.11824(31)	1	0.047(4)
	80947		1/3	2/3	0.11824(21)	1	0.013(32)
Interlayer							
C1	10604	2d	2/3	1/3	¼	0.0625*	0.01(2)
			2/3	1/3	¼	0.0625*	0.023(3)
C2	10604	2b	0	0	¼	0.0625*	0.012(23)
	80947		0	0	¼	0.0625*	0.01(2)
O2	10604	6h12j	0.44637(49)	0.55463(49)	¼	0.0625*22(4)	0.0321(8)
	80947		0.4458(86)	0.5552(86)	¼	0.17(4)0.0625*	0.0183(15)
O3	10604	6h12j	0.22819(61)	0.4638(21)	¼	0.0625*18(4)	0.0196(15)
	80947		0.22217(85)	0.0434(21)	¼	0.0625*21(7)	0.0194(15)
Anisotropic displacement parameters of atoms in octahedral layer							
Atom	Crystal	U_{11}	U_{22}	U_{33}	U_{23}	U_{13}	U_{12}
*M*1	10604	0.008(1)0.0066(7)	= U_{11}	0.017(1)0.015(1)	0	0	0.0038(5)0.0033(4)
	80947	0.004229(89)	= U_{11}	0.0120(1)	0	0	0.002115(4)
O1	10604	0.016(1)0.016(1)	= U_{11}	0.014(2)0.013(1)	0	0	0.015(1)0.0081(6)
	80947	0.012(1)	= U_{11}	0.011(2)	0	0	0.00623(6)

* fixed during refinement

667

668 **Table 5**. Selected bond lengths (Å) in the structure of hydrotalcite-3*R* and hydrotalcite-2*H*

669

Hydrotalcite-3*R*				Hydrotalcite-2*H*		
Sample number	9699	9699 LT	Kir4940	Sample number	10604	80947
*M*1-O × 6	2.039(1)	2.033(1)	2.031421(96)	*M*1-O × 6	2.0212(2)	2.027(2)
C1-O2 × 3	1.2917(81)	1.2846(81)	1.300283(87)	C1-O2 × 3	12.2216(25)	1.176(43)
C1-O3 × 3	1.775(2)	1.7677(3)	1.7685(5)	C2-O3 × 3	1.2002(37)*	1.175(53)

Hydrogen bonding scheme

Sample №	**D**-H**	d(**D**-H)	d(H···**A**)	<**D**H**A**	d(**D**···**A**)	**A**
3*R*						
9699	O1-H1	0.815	2.152	163.82	2.943	O2
9699 LT	O1-H1	0.819	2.131	163.66	2.925	O2
Kir4940	O1-H1	0.821	2.145	164.19	2.944	O2
2*H*						
10604	OH1-H1	0.817	2.131	164.88	2.927	O3
	OH1-H1	0.817	2.142	163.83	2.935	O2
80947	OH1-H1	0.815	2.128	163.89	2.919	O3
	OH1-H1	0.815	2.128	163.87	2.919	O2

670

671 * the C-O distance is fixed at 1.21(5) Å

672 ** the O-H distance is fixed at 0.82(2) Å

673

Table 6. Hydrotalcite-supergroup minerals comprising $\sqrt{3} \times \sqrt{3}$ superstructure due to long-range ordering of M^{2+} and M^{3+} (M^{2+}:M^{3+} = 2:1) within metal -hydroxide layer

Mineral name	Chemical formula	Crystal system	Unit-cell parameters[1]				Refe-rence
			a	*b*	*c*	ß	
			Å			°	
Quintinite-2*T*-3*c*	$[Mg_4Al_2(OH)_{12}][(CO_3)(H_2O)_3]$	Trigonal	5.27	= *a*	45.36	90	(1)
Quintinite-2*T*		Trigonal	5.28	= *a*	15.15	90	(2)
			5.27	= *a*	15.11	90	(3)
Quintinite-1*M*		Monoclinic	5.27	9.11	7.77	103.2	(4)
			5.28	9.15	7.76	103.0	(5)
			5.23	9.05	7.71	103.1	(6)
Shigaite	$[Mn_6Al_3(OH)_{18}][Na(H_2O)_6][SO_4]_2(H_2O)_6$	Trigonal	9.51	= *a*	33.07	90	(7)
Nikischerite	$[Fe^{2+}{}_6Al_3(OH)_{18}][Na(H_2O)_6][SO_4]_2(H_2O)_6$	Trigonal	9.35	= *a*	33.00	90	(8)
Cualstibite	$[Cu_2Al(OH)_6][Sb(OH)_6]$	Trigonal	9.20	= *a*	9.80	90	(9)
		Trigonal	9.15	= *a*	9.74	90	(10)
		Monoclinic	9.94	8.90	5.49	102.9	(11)
Zincalsibite	$[Zn_2Al(OH)_6][Sb(OH)_6]$	Trigonal	5.33	= *a*	9.79	90	(12)
		Trigonal	5.34	= *a*	88.01	90	(13)
Omsite	$[Ni_2Fe^{3+}(OH)_6][Sb(OH)_6]$	Trigonal	5.35	= *a*	19.58	90	(14)
Hydrocalumite	$[Ca_4Al_2(OH)_{12}][(Cl,CO_3,OH)_{2-x}(H_2O)_4]$	Monoclinic	10.02	11.50	16.29	104.2	(15)
Kuzelite	$[Ca_4Al_2(OH)_{12}][SO_4]_2(H_2O)_6$	Trigonal	5.76	= *a*	26.80	90	(16)

[1] numbers are rounded for the sake of simplicity

(1) Krivovichev *et al*., 2010a, (2) Arakcheeva *et al*., 1996, (3) Zhitova *et al*., 2018a, (4) Krivovichev *et al*., 2010b, (5) Krivovichev *et al*., 2012, (6) Zhitova *et al*., 2018b, (7) Cooper and Hawthorne, 1996, (8) Huminicki and Hawthorne, 2003, (9) Walenta, 1984, (10) Bonaccorsi *et al*., 2007, (11) Kolitsch *et al*., 2013, (12) Bonaccorsi *et al*., 2007, (13) Mills *et al*., 2012*b*, (14) Mills *et al*., 2012*c*, (15) Sacerdoti and Passaglia, 1988, (16) Allmann, 1977.